Journal of Materials Chemistry A

Accepted Manuscript

ROYAL SOCIETY OF CHEMISTRY

www.rsc.org/materialsA

Cite this: DOI: 10.1039/c0xx00000x

www.rsc.org/xxxxxx

ARTICLE TYPE

Ammonia Borane Confined by Nitrogen-containing Carbon Nanotubes: Enhanced Dehydrogenation Properties Originating from the Synergetic Catalysis and Nanoconfinement

Lijun Zhang,[a] Guanglin Xia[b] Yu Ge[d], Caiyun Wang[d], Zaiping Guo[b]*, Xingguo Li[c] and Xuebin Yu[a]*

Received (in XXX, XXX) Xth XXXXXXXXX 20XX, Accepted Xth XXXXXXXXX 20XX
DOI: 10.1039/b000000x

Borane−amine adducts ($H_3N{\cdot}BH_3$, AB) in tetrahydrofuran solution were infiltrated into polypyrrole (PPy) nanotubes by a capillary effect, forming an ammonia borane (AB)@PPy combined system. This composite system combines the synergetic catalysis of nitrogen atoms with nanoconfinement in nanotubes, resulting in a significant improvement in the dehydrogenation properties. Dehydrogenation results showed that the AB loaded on PPy can release 15.3% hydrogen below 150 °C with an onset decomposition temperature as low as 48 °C. More importantly, the evolution of harmful ammonia, diborane, and borazine was entirely suppressed.

Introduction

In the endeavor to decrease greenhouse gas emissions and fossil fuel dependence, hydrogen has been considered as one of the best alternative energy carriers because of its abundance, high energy density, and environmental friendliness.[1] Highly efficient and convenient hydrogen storage materials/technology are still the main challenge for today's development of the hydrogen economy.[2-4] The chemical storage of hydrogen in solid or liquid compounds from which it can be released as gas through a suitable dehydrogenation reaction has been intensively investigated as a possibility to overcome some of these challenge.[5, 6] Methanol belongs to the broader class of liquid storage compounds which includes liquid organic hydrogen carriers. It is a key platform chemical for existing fuel and chemical infrastructures and contains 12.6% hydrogen, which can be released through aqueous reforming. Heterogeneous catalysts, which promote this reaction and the reverse one, the conversion of CO_2 and H_2 to MeOH, operate at high temperatures (>200 °C) and applied pressures (>25 bar).[7] Indeed the high temperature required for dehydrogenation is one of the main factors which so far has made MeOH less suitable as energy carrier in the field of portable applications.[8] Therefore, developing milder routes is highly desirable in order to reach a viable H_2 energy system. Recently, extensive efforts have been focused on storing H_2 in chemical bonds in condensed phase materials,[9, 10] for instance, boron–nitrogen–hydrogen (B-N-H) compounds,[11, 12] which contain both protic (N-H) and hydridic (B-H) hydrogen atoms and allow a facile H_2 elimination pathway,[13] providing high gravimetric hydrogen capacities at relatively low temperature.[14-21] Among these B-N-H compounds, the parent ammonia borane (AB) has attracted great interest as an H_2-vector for chemical hydrogen storage because of the following advantages: (i) high gravimetric hydrogen storage capacity (19.6 wt%); (ii) low molecular weight (30.7 $g{\cdot}mol^{-1}$); and (iii) it is non-flammable and non-explosive under standard conditions.[22-27] The exothermic nature of AB dehydrogenation renders thermal degradation the simplest approach. Despite the fact that AB can release > 12 wt.% H_2 over the temperature range from 90-150 °C with a kinetically controlled decomposition, its practical application is still frustrated by some crucial issues, such as poor reversibility, slow kinetics at low temperatures (below 90 °C), and excessive volatile impurities (borazine, diborane and ammonia) during dehydrogenation. [25, 28, 29]

To overcome the above drawbacks, much research has been conducted on investigating the thermal decomposition of AB, including with hydrolysis,[28] transition metal[30-32] or acid-base catalysts[22], chemical modification of AB through replacing one of its H atoms with another element to form derivatives, etc.[33-35] Nanoconfinement by nanoscaffolds[36] has also been demonstrated to be an effective route to improve the dehydrogenation properties of AB.[30, 37-41] A pioneering work by Autrey and co-workers found that the dehydrogenation kinetics and thermodynamics of AB were improved after an internal coating of AB was applied in nanoscaffolds (SBA–15) using methanol as solvent.[42] Meanwhile, Cao *et al.* lowered the activation energy of AB and suppressed the emission of harmful by-products by dissolving AB in tert-butyl alcohol and spreading it into carbon cryogels and BN-modified carbon cryogels.[37] Our recent results suggest that nitrogen-containing carbon nanostructures (NCCN) can serve as excellent metal-free catalysts for facilitating the hydrogen release of AB with relatively low energy barriers.[43] For example, mesoporous graphitic carbon nitride[24] and triazine-based frameworks[43] can serve as strong Lewis base sites that effectively catalyze the dehydrogenation of AB and produce cross-linked polyborazylene (PB) as the single spent-fuel component, which significantly improves the dehydrogenation of AB. This suggests that electron-accepting nitrogen atoms incorporated into various carbon nanostructures may serve as highly active carriers in destabilizing the bonds in AB, due to the strong electron affinity of the nitrogen atoms in the nanostructures, and thus catalyse the release of pure H_2 from AB

at relatively low temperatures. In this regard, carbon nanostructures doped with appropriate heteroatoms appear to hold considerable promise as effective AB dehydrogenation catalysts.

In this paper, as schematically illustrated in Scheme 1, the AB was incorporated into polypyrrole (PPy) nanotubes to form an AB@PPy combined system by a wet chemical route. AB@PPy combines the synergetic catalysis of PPy and of nitrogen atoms, as well as offering nanoconfinement in nanotubes, resulting in a significantly improved dehydrogenation of AB. These findings establish a promising approach via utilizing PPy as metal-free catalysts and nanoscaffolds for the dehydrogenation of ammonia borane and other related boron–nitrogen species.

Scheme 1 Illustration of the preparation of AB confined in PPy.

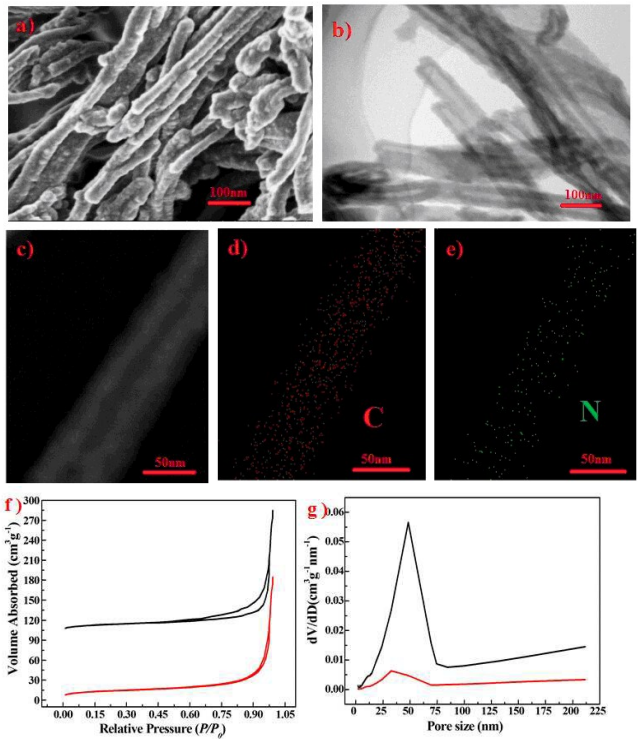

Fig. 1 SEM (a) and TEM (b) micrographs of PPy; TEM image (c) of a single PPy nanotube, and the corresponding EDX maps of the elements C (d) and N (e); N_2 sorption isotherms (f) and pore size distributions (g) for the pure PPy (black line) and AB@PPy (red line).

Fig. 1a shows a typical scanning electron microscope (SEM) image of PPy nanotubes with smooth surfaces and diameters around 50–60 nm. The transmission electron microscope (TEM) image in Fig. 1b shows that PPy possesses a hollow nanotube structure with a large internal hollow space. The thickness of the carbon layer was estimated to be around 10 nm. This structure in principle allows for high dispersion of bulk materials and fine control of the compounds within nanochannel pores. The energy dispersive spectroscopy (EDS) results reveal that the C and N maps agree well with the structure of the PPy nanotubes (Fig. 1c-e). Nitrogen adsorption measurements (Fig. 1f) exhibit type IV isotherm behaviour with H_3 hysteresis, implying that the PPy nanotubes are mesoporous with a Brunauer-Emmett-Teller (BET) surface area of 74.9 $m^2 \cdot g^{-1}$. The distribution of Barrett-Joyner-Halenda (BJH) pore sizes (Fig. 1g) determined from the adsorption branches peaks at 40 nm. The PPy used in this work shows not only the aforementioned properties, i.e. relatively large usable loading area, suitable average pore diameter, and high thermal stability upon heating to 200 ^oC (Fig. S1 in the Supporting Information), but also the ability to swell when immersed in polar solvents because of its abundant hydrogen bonds. This ability is particularly beneficial for the solubilized impregnation of bulk materials, which was exploited by us here to load the hydrogen storage material AB.

As shown in Fig. 2a and 2b, the obtained AB@PPy retained similar morphology to pure PPy, while the surface became rough, and the diameters of the nanotubes were enlarged up to 60–70 nm, resulting in partial loading of AB on the surface of the PPy. The energy dispersive X-ray spectroscopy (EDX) element maps in Fig. 3d-g confirm that the C, N, and B coincide very well with the structure of PPy, demonstrating the high dispersion of AB in the PPy framework. The SEM and TEM-EDX results support the assertion that AB was encapsulated into the PPy nanotubes as well as uniformly covering its surface, forming an embedded nanocomposite structure. In addition, the BET analysis shows that, compared with the as-prepared PPy, the space-confined AB@PPy has a reduced intensity in its pore size distribution and a smaller peak size of 30 nm (Fig. 1f). Both the BET specific surface area and the BJH total pore volume are decreased from 74.9 to 5.3 $m^2 \cdot g^{-1}$ and from 0.29 to 0.06 $cm^3 \cdot g^{-1}$, respectively. These results further confirm that the PPy pores are filled by the AB. The structures of the pristine AB, the sample of AB mixed with PPy, the AB@PPy sample, and the pure PPy characterized by powder X-ray diffraction (XRD, Fig. S2). The XRD patterns show that the AB mixed with PPy shows sharp peaks with 2θ of 22.5-25° and 33-35°, which are assigned to pure AB, implying that the AB did not decompose or react with the PPy during the physical mixing process. In contrast, only a broad peak between 20° and 30° belonging to pure PPy was observed for the AB@PPy, indicating that AB was formed in the amorphous state in the composite.

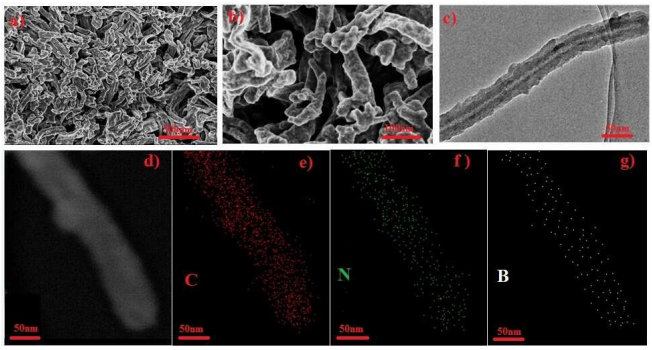

Fig. 2 SEM (a, b) images under different magnifications, and TEM (c) image of AB@PPy; TEM image (d) of a single AB@PPy nanotube, and the corresponding EDX maps of the elements C (e), N (f), and B (g).

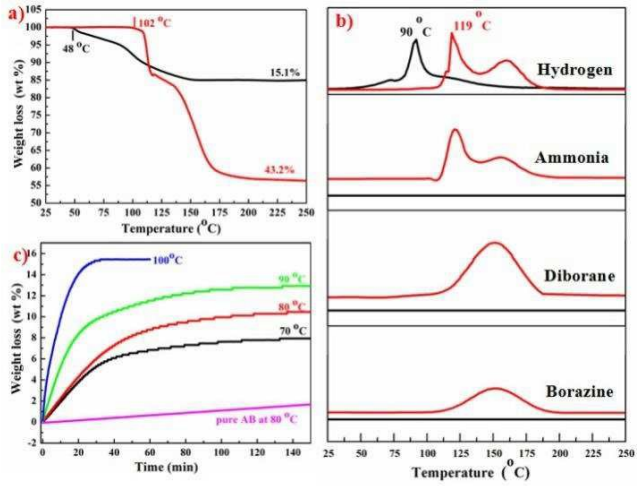

Fig. 3 TG (a) and MS (b) results for AB@PPy (black line) and neat AB (red line), with a heating rate of 5 ^{o}C·min^{-1} in nitrogen. (c) Isothermal dehydrogenation results for AB@PPy at 70, 80, 90, and 100 ^{o}C, and neat AB at 80 ^{o}C.

The comparative decomposition properties of neat AB and the AB@PPy combined system determined via thermogravimetry (TG), mass spectroscopy (MS), and temperature programmed desorption (TPD) measurements over the temperature range from 25 to 250 ^{o}C with a heating rate of 5 ^{o}C min^{-1} are shown in Figs. 3 and S3. As shown in Fig. 3a, it is evident that neat AB starts to decompose slightly above 100 ^{o}C via a two-step process, and the weight loss reaches 43.2 wt%,[44] which is much larger than the theoretical hydrogen release capacity in AB (19.6%) due to the release of hydrogen accompanied by volatile impurities (NH_3, B_2H_6, and borazine), as demonstrated by the MS characterization (Fig. 3b). The onset decomposition of AB@PPy, however, starts at about 48 ^{o}C, with the first dehydrogenation peak centered at 90 ^{o}C, which is about 30 ^{o}C lower than that of neat AB. Furthermore, the MS results in Fig. 3b show that there is only hydrogen released from AB@PPy, while the emission of ammonia, diborane, and borazine was completely suppressed. This is also verified by the TG result (Fig. 3b), which gives a total weight loss of 15.1 wt.% for AB@PPy below 150 ^{o}C. The TPD measurements (Fig. S3a) show that the amount of hydrogen released from AB@PPy is nearly the same as in the TG result, further confirming the pure hydrogen release in AB@PPy. A comparison of impurity gas and dehydrogenation temperature of AB incorporated by PPy and other supporters reported (Table S1) shows that AB@PPy exceed the other size-confined systems. This result further clarifies that the synergetic catalysis of PPy and of nitrogen atoms, as well as hybrid effect of size-confinement facilitate pure H_2 generation from AB. The isothermal dehydrogenation results in Fig. 3c show that little hydrogen evolution from the neat AB is observable at 80 ^{o}C within 30 min. In contrast, the AB@PPy nanocomposite generates 15.5, 9.75, 6.01, and 5.18 wt% H_2 at 100, 90, 80, and 70 ^{o}C within 30 min. For a better exploration of the kinetic properties, the activation energies of AB and AB@PPy were estimated from various isotherm curves through the Arrhenius treatment. Compared with the 183 kJ·mol^{-1} for neat AB,[44] the apparent activation energy for H_2 loss from AB@PPy were was decreased to 78.5 kJ·mol^{-1}, distinctly validating the kinetic enhancement in AB@PPy.

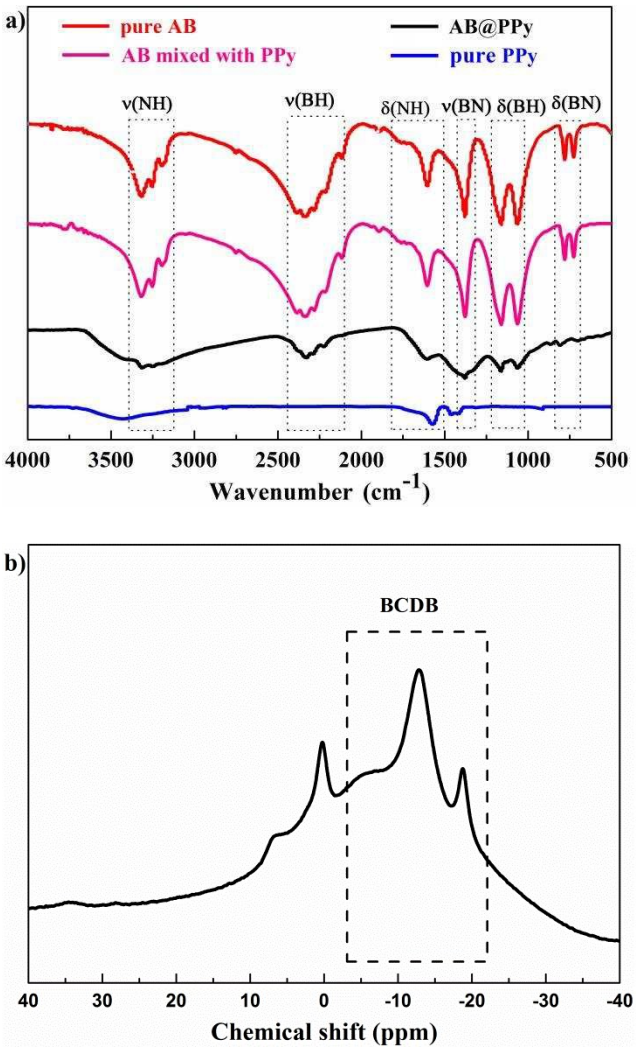

Fig. 4 a) FTIR spectra for pure AB, AB mixed with PPy, AB@PPy, and pure PPy. b) Solid-state ^{11}B NMR spectrum of AB@PPy composite after release of 1 equiv. H_2.

To gain insight into the dehydrogenation process, Fourier transform infrared (FTIR) and ^{11}B nuclear magnetic resonance (NMR) measurements were conducted. The FTIR results for neat AB, AB mixed with PPy, AB@PPy, and pure PPy are shown in Fig. 4a. When AB is physically mixed with PPy, the vibrations assigned to B–H, N–H, and B–N remain almost unchanged, implying that there is almost no force between AB and PPy in such circumstances. The NMR result in Fig. 4b shows that, after releasing one equiv. H_2 from the AB@PPy, apparent resonance peaks at –5.3, –12.8, and –18.9 ppm are observed, corresponding to B-(cyclodiborazanyl)-aminoborohydride (BCDB),[45, 46] suggesting that PPy can catalyze the decomposition of AB, yielding linear NH_2BH_2. The resonance peaks at 0 ppm may be attributable to partial oxidation of the sample during the measurement process. In our previous studies,[43] a series of first-principles calculations based on density functional theory (DFT) were performed to understand the interaction between AB and NCCN. They revealed that the incorporation of electron-accepting nitrogen atoms into conjugated carbon nanostructures plays a crucial role in enhancing the binding strength between AB and the carbon nanostructures, thus allowing metal-free hydrogen transfer from AB to NCCN via an asynchronous concerted process with the N-to-N protic transfer promoted over the B-to-N hydridic transfer in the transition state. Then, the hydrogenated NCCN further reacts with AB to release H_2 with relatively low reaction barriers compared to those of pristine AB. As PPy is one kind of NCCN, AB@PPy may experience the following dehydrogenation mechanism, as illustrated in Scheme 2. Firstly, one hydrogen ion (proton) of AB is transferred to PPy, forming two intermediates. Then, the two intermediates react with each other, releasing one molecule of hydrogen, with the result that PPy recovers its structure and the linear NH_2BH_2 is formed, as confirmed by the NMR results.

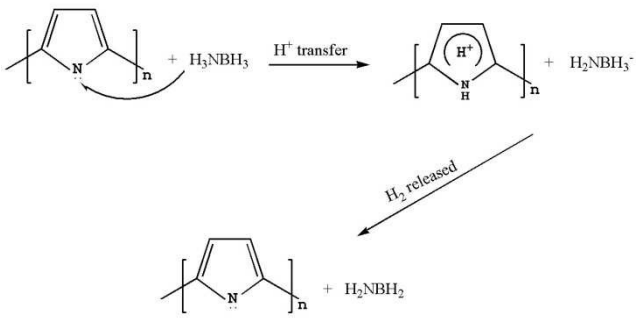

Scheme 2 Possible dehydrogenation mechanism of AB@PPy.

Conclusions

PPy nanotubes have been used as nanoscaffolds for AB in order to improve its dehydrogenation properties. The as-formed AB@PPy is able to liberate H_2 at temperatures as low as 48 °C, and up to 15.3 wt % pure hydrogen can be released before 150 °C without any harmful impurities. This improvement is ascribed to the synergistic effects of nanoconfinement and N-catalysis. Our results suggest that AB@PPy composite material is a safe potential hydrogen storage material.

Experimental sections

Reagents and synthesis

Pyrrole was purchased from Merck and was freshly distilled before use. All the other chemicals were obtained from Sigma-Aldrich and used as-supplied. The PPy nanotubes were synthesized using methyl orange (MO) as template.[47] In a typical procedure, 0.405 g $FeCl_3 \cdot 6H_2O$ was added into 30 mL of 5 mM MO aqueous solution, with flocculent precipitate observed immediately. Then, 105 μL (1.5 mmol) pyrrole monomer was added into the above suspension, and the mixture was stirred at room temperature for 24 h, forming a black precipitate. The PPy nanotubes were obtained by rinsing the black product with deionized water and ethanol until the filtrate was colourless and then vacuum-drying it at 60 °C for 12 h. The AB@PPy sample was prepared by solvent infiltration of AB in tetahydrofuran (THF) solution into PPy nanotubes. In a typical experiment, AB (350 mg) was dissolved in THF (6 ml, distilled before use) at room temperature, and the saturated solution of AB in THF was added to a sample of PPy (700 mg) using a syringe. The THF solution appeared to fill the internal channels of the nanoporous scaffold immediately through immersion. The mixture of AB solution and PPy was further sonicated for about 4 h at 0 °C to

obtain homogeneous, finely dispersed AB@PPy. Finally, the sample was exposed to vacuum at room temperature for 4 h to remove the THF, leading to the formation of the AB@PPy sample with a mass ratio of 1:2.

Instrumentation and analysis

The high-resolution synchrotron powder X-ray diffraction data were collected by a Mythen-II detector with a wavelength of λ = 1.0315 Å at the Powder Diffraction Beamline, Australian Synchrotron. Fourier transform infrared (FTIR) spectroscopy (Magna-IR 550 II, Nicolet) was conducted to determine the chemical bonds. Samples were pressed with KBr and then loaded into a sealed chamber filled with argon to be measured. Thermal property measurements were performed by thermogravimetry (TG, STA 409C)/mass spectroscopy (MS, QMS403) with a heating rate of 5 °C min^{-1} under 1 bar argon. Dehydrogenation properties for the samples were evaluated using Sievert's volumetric method with a heating rate of 5 °C min^{-1} under argon. Approximately 0.03 g of the sample was loaded and heated with a heating rate of 5 °C min^{-1} from room temperature to 250 °C. The pressure data (*P*) and the temperature data (*T*) were recorded automatically at every other 6 s. Finally, according to the equation: $PV = nRT$, where *R* is the gas constant, the moles (*n*) of gas released from the sample could be calculated. Solid-state ^{11}B-NMR results were collected on a Bruker Avance 300 MHz spectrometer, using a Doty CP-MAS probe with no probe background. The powder samples collected after the decomposition reaction were spun at 5 kHz, using 4 mm ZrO_2 rotors filled up in a purified argon atmosphere glove box. 0.55 μs single-pulse excitation was employed, with repetition time of 1.5 s. The microstructures were observed by transmission electron microscopy (TEM, JEM-2100F, JEOL) and field-emission scanning electron-microscopy (SEM, S-4800, Hitachi).

Acknowledgements

This work was partially supported by the National Natural Science Foundation of China (21271046, 51471053) and the PhD Programs Foundation of the Ministry of Education of China (20110071110009). Funding from the Australian Research Council Centre of Excellence Scheme (Project Number CE 140100012) is also gratefully acknowledged. The authors would like to thank the Australian National Nanofabrication Facility-Materials node (ANFF) and the UOW Electron Microscopy Centre for the use of equipment, and thank Dr. Tania Silver for critical reading of the manuscript.

Notes and references

[a] Department of Materials Science, Fudan University, Shanghai, China.
E-mail: yuxuebin@fudan.edu.cn
[b] Institute for Superconducting and Electronic Materials, University of Wollongong, Wollongong, Australia. E-mail: zguo@uow.edu.au
[c] College of Chemistry and Molecular Engineering, Peking University, Beijing 100871, P. R. China.
[d] Intelligent Polymer Research Institute, ARC Centre of Excellence for Electromaterials Science, University of Wollongong, Australia.

† Electronic Supplementary Information (ESI) available: TG, XRD, and TPD results.

1. L. Schlapbach and A. Zuttel, *Nature*, 2001, **414**, 353-358.
2. W. Grochala and P. P. Edwards, *Chem. Rev.*, 2004, **104**, 1283-1315.
3. J. Graetz, *Chem. Soc. Rev.*, 2009, **38**, 73-82.
4. M. Bechelany, A. Abou Chaaya, F. Frances, O. Akdim, D. Cot, U. B. Demirci and P. Miele, *J. Mater. Chem. A*, 2013, **1**, 2133-2138.
5. E. Balaraman, C. Gunanathan, J. Zhang, L. J. W. Shimon and D. Milstein, *Nature Chemistry*, 2011, **3**, 609-614.
6. E. Alberico and M. Nielsen, *Chem. Commun.*, 2015, **51**, 6714-6725.
7. E. Balaraman, Y. Ben-David and D. Milstein, *Angew. Chem. Int. Ed.*, 2011, **50**, 11702-11705.
8. E. Alberico, P. Sponholz, C. Cordes, M. Nielsen, H.-J. Drexler, W. Baumann, H. Junge and M. Beller, *Angew. Chem. Int. Ed.*, 2013, **52**, 14162-14166.
9. H. W. Li, Y. G. Yan, S. Orimo, A. Zuttel and C. M. Jensen, *Energies*, 2011, **4**, 185-214.
10. H. W. Li, Y. G. Yan, E. Akiba and S. Orimo, *Mater. Trans.*, 2014, **55**, 1134-1137.
11. R. Moury, U. B. Demirci, V. Ban, Y. Filinchuk, T. Ichikawa, L. Zeng, K. Goshome and P. Miele, *Chem. Mater.*, 2014, **26**, 3249-3255.
12. G. Moussa, U. B. Demirci, S. Malo, S. Bernard and P. Miele, *J. Mater. Chem. A*, 2014, **2**, 7717-7722.
13. R. Moury and U. B. Demirci, *Energies*, 2015, **8**, 3118-3141.
14. S.-i. Orimo, Y. Nakamori, J. R. Eliseo, A. Zuettel and C. M. Jensen, *Chem. Rev.*, 2007, **107**, 4111-4132.
15. M. E. Bluhm, M. G. Bradley, R. Butterick, U. Kusari and L. G. Sneddon, *J. Am. Chem. Soc.*, 2006, **128**, 7748-7749.
16. Y. Guo, X. Yu, W. Sun, D. Sun and W. Yang, *Angew. Chem. Int. Ed.*, 2011, **50**, 1087-1091.
17. Y. Guo, H. Wu, W. Zhou and X. Yu, *J. Am. Chem. Soc.*, 2011, **133**, 4690-4693.
18. Q. Gu, L. Gao, Y. Guo, Y. Tan, Z. Tang, K. S. Wallwork, F. Zhang and X. Yu, *Energy Environ. Sci.*, 2012, **5**, 7590-7600.
19. W. Luo, P. G. Campbell, L. N. Zakharov and S.-Y. Liu, *J. Am. Chem. Soc.*, 2011, **133**, 19326-19329.
20. W. C. Ewing, A. Marchione, D. W. Himmelberger, P. J. Carroll and L. G. Sneddon, *J. Am. Chem. Soc.*, 2011, **133**, 17093-17099.
21. H. Fu, J. Yang, X. Wang, G. Xin, J. Zheng and X. Li, *Inorg. Chem.*, 2014, **53**, 7334-7339.
22. F. H. Stephens, R. T. Baker, M. H. Matus, D. J. Grant and D. A. Dixon, *Angew. Chem. Int. Ed.*, 2007, **46**, 746-749.
23. Z. Tang, H. Chen, X. Chen, L. Wu and X. Yu, *J. Am. Chem. Soc.*, 2012, **134**, 5464-5467.
24. Z. Tang, X. Chen, H. Chen, L. Wu and X. Yu, *Angew. Chem. Int. Ed.*, 2013, **52**, 5832-5835.
25. A. C. Stowe, W. J. Shaw, J. C. Linehan, B. Schmid and T. Autrey, *Phys. Chem. Chem. Phys.*, 2007, **9**, 1831-1836.
26. T. B. Marder, *Angew. Chem. Int. Ed.*, 2007, **46**, 8116-8118.
27. J. Zhao, J. Shi, X. Zhang, F. Cheng, J. Liang, Z. Tao and J. Chen, *Adv. Mater.*, 2010, **22**, 394-397.

28. Q.-L. Zhu and Q. Xu, *Energy Environ. Sci.*, 2015, **8**, 478-512.
29. H. Kim, A. Karkamkar, T. Autrey, P. Chupas and T. Proffen, *J. Am. Chem. Soc.*, 2009, **131**, 13749-13755.
30. S. F. Li, Y. H. Guo, W. W. Sun, D. L. Sun and X. B. Yu, *J. Phys. Chem. C*, 2010, **114**, 21885-21890.
31. C. A. Jaska, K. Temple, A. J. Lough and I. Manners, *J. Am. Chem. Soc.*, 2003, **125**, 9424-9434.
32. J.-M. Yan, X.-B. Zhang, S. Han, H. Shioyama and Q. Xu, *Angew. Chem. Int. Ed.*, 2008, **47**, 2287-2289.
33. L. Zhang, S. Li, Y. Tan, Z. Tang, Z. Guo and X. Yu, *J. Mater. Chem. A*, 2014, **2**, 10682-10687.
34. L. Li, Q. Gu, Z. Tang, X. Chen, Y. Tan, Q. Li and X. Yu, *J. Mater. Chem. A*, 2013, **1**, 12263-12269.
35. H.-W. Li, E. Akiba and S.-i. Orimo, *J. Alloy. Compd.*, 2013, **580**, S292-S295.
36. Z. Li, G. Zhu, G. Lu, S. Qiu and X. Yao, *J. Am. Chem. Soc.*, 2010, **132**, 1490-1491.
37. S. Sepehri, B. B. Garcia and G. Cao, *Eur. J. Inorg. Chem.*, 2009, 599-603.
38. Z. Tang, S. Li, Z. Yang and X. Yu, *J. Mater. Chem.*, 2011, **21**, 14616-14621.
39. Y. Li, L. Xie, Y. Li, J. Zheng and X. Li, *Chem-eur. J.*, 2009, **15**, 8951-8954.
40. L. Li, X. Yao, C. Sun, A. Du, L. Cheng, Z. Zhu, C. Yu, J. Zou, S. C. Smith, P. Wang, H.-M. Cheng, R. L. Frost and G. Q. Lu, *Adv. Funct. Mater.*, 2009, **19**, 265-271.
41. A. Feaver, S. Sepehri, P. Shamberger, A. Stowe, T. Autrey and G. Cao, *J. Phys. Chem. B*, 2007, **111**, 7469-7472.
42. A. Gutowska, L. Y. Li, Y. S. Shin, C. M. M. Wang, X. H. S. Li, J. C. Linehan, R. S. Smith, B. D. Kay, B. Schmid, W. Shaw, M. Gutowski and T. Autrey, *Angew. Chem. Int. Ed.*, 2005, **44**, 3578-3582.
43. X. Chen, L. Wan, J. Huang, L. Ouyang, M. Zhu, Z. Guo and X. Yu, *Carbon*, 2014, **68**, 462-472.
44. X. Kang, Z. Fang, L. Kong, H. Cheng, X. Yao, G. Lu and P. Wang, *Adv. Mater.*, 2008, **20**, 2756-2759.
45. X. Yang, L. Zhao, T. Fox, Z.-X. Wang and H. Berke, *Angew. Chem. Int. Ed.*, 2010, **49**, 2058-2062.
46. W. J. Shaw, J. C. Linehan, N. K. Szymczak, D. J. Heldebrant, C. Yonker, D. M. Camaioni, R. T. Baker and T. Autrey, *Angew. Chem. Int. Ed.*, 2008, **47**, 7603-7606.
47. E. M. I. M. Ekanayake, D. M. G. Preethichandra and K. Kaneto, *Biosens. Bioelectron.*, 2007, **23**, 107-113.

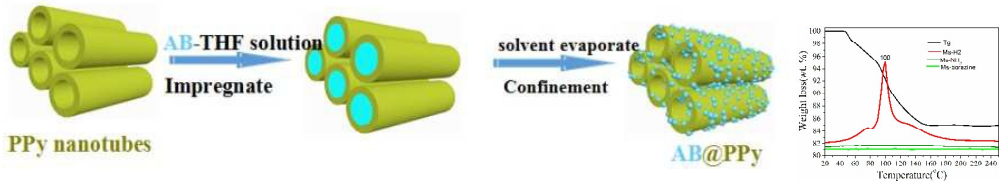

AB@PPy composites synthesized by a solution method show favorable dehydrogenation properties.